DEVELOPMENT OF STATE OF THE ART INSTRUMENTATION TO MEASURE DIELECTRIC BREAKDOWN VOLTAGE OF INSULATING LIQUIDS AND MEASURING THE ABILITY OF AN INSULATING LIQUIDS TO WITHSTAND ELECTRICAL STRESS

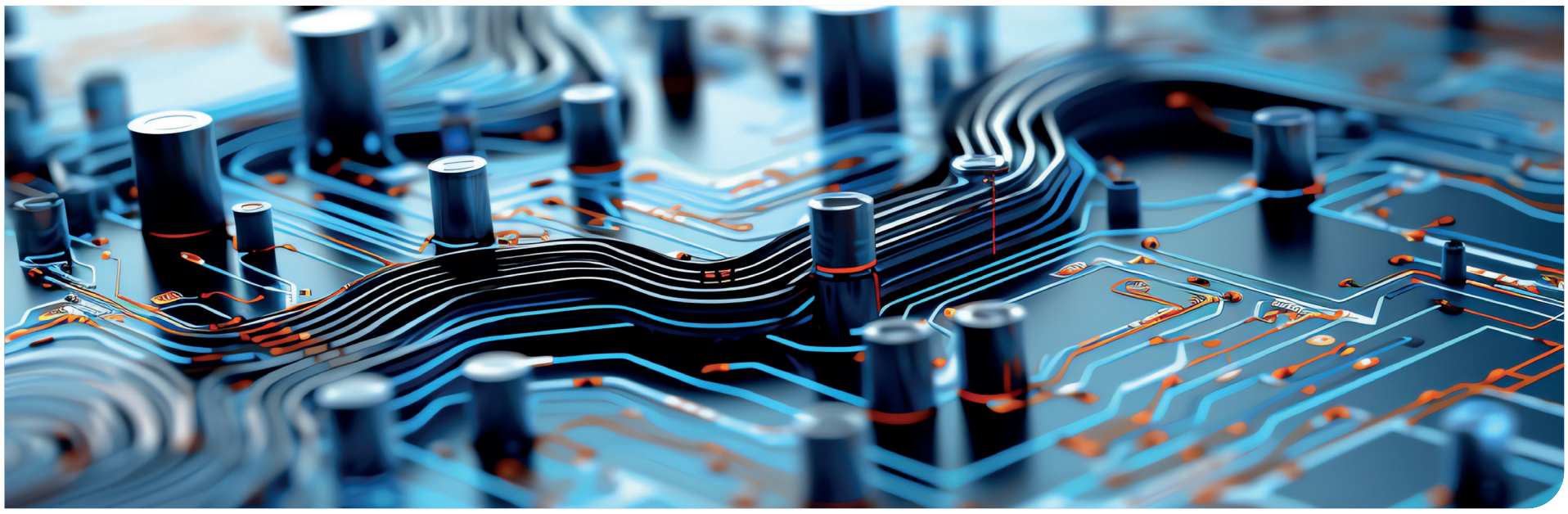

Introduction

In 1745, German physicist Ewald Georg von Kleist, pioneer of the dielectric, discovered that water could store charges with his Leyden Jar invention, a hand-sized jar filled with water wired to a high voltage generator, and coined the term dielectric to any form of insulating matter that could barricade the flow of current.[1] Upon experiencing an applied electric field by the current, dielectric materials undergo microscopic polarization, an activity that aids its ability to store electrical energy and an exclusive property within the classification of insulators.[2] Its distinctive nature permits ubiquitous applications in conductors, microelectronics, lithography, etching, and energy production amongst other fields. [3] However, dielectrics break down at high voltages, causing hazardous ionization of surrounding substances or equipment malfunctions. As a result, dielectric machines should be exercised with caution, as they are far from impenetrable.[4] Here, we will explore the modern applications of dielectrics and dielectric breakdowns, the physical chemistry behind dielectric breakdowns, and the ASTM testing method for dielectric breakdown voltage of insulating liquids.

Dielectric Applications and Breakdown Mechanism

Dielectric breakdown transpires upon surpassing a material's dielectric strength or the maximum electric field a material can withstand. Once the dielectric begins disintegration at breakdown voltage, the material relinquishes its insulating properties and conducts electricity. Dielectric breakdown applies to gasses, liquids, and solids, only requiring two major components: carrier injection of electrons and impact ionization. The insulating material is placed between the gap between two electrodes (an anode and a cathode) connected to a high voltage source that executes the flow of current. In any material, there are two energy bands electrons may occupy: the valence and the higher-energy conduction band. Once the electrons in the dielectric material receive sufficient energy from the applied electric field, they will ascend to the conduction band and act as mobile charge carriers. The cathode houses these electrons that will bombard the anode surface, freeing positive ions at the anode surface while generating metallic vapor. These positive ions then bombard the cathode surface and launch a second wave of electron emissions while also producing metallic vapor, ultimately revving up a cycle of charged particle collisions until breakdown occurs. Impact ionization arises during this bombardment cycle, referring to a process in which stimulated electrons collide with molecules in the dielectric material and free their electrons. For gasses, ionization begins at the metallic vapors released from the bombardment of charged particles, resulting in sparks or openings for the passing of current. In liquids, bubbles form instead and act as the sites for ionization. These bubbles grow alongside the rapid cycling of electrons until breakdown occurs. In solids, deterioration of the dielectric material stems from electrical aging and eventual breakdown. Consequently, the dielectric breakdown strength is vastly contingent upon electrode material, microstructure of the dielectric material, and contaminants in the dielectric material. [4] [5]

Applications of dielectrics (i.e. glass, parylene, ceramics, and mineral oils) include increasing capacitor strength, isolating semiconductor components, generating stable wave frequencies in resonance oscillators, and acting as commercial coating agents against corrosions and chemicals..[4] Thus, being informed about the breakdown voltage of a dielectric material is integral, especially in preventing electric shocks, fire hazards, short circuits, blown fuses, or irreversible damage to equipment. Nonetheless, well-intended dielectric breakdowns can be advantageous too, especially in fuel ignition devices. Cigarette lighters, for example, utilize the dielectric breakdown of air to trigger a sustaining flame without any external sources by creating a spark in between electrode gaps and igniting the fuel beneath.[5] Other beneficial applications of dielectric breakdowns, including titanium coating oxidation and cryptographic key generation, will be discussed later in this paper.

ASTM 877

ASTM 877 discerns the electric breakdown voltage or the ability to undergo electrical stress of unfiltered or gassed insulating liquids using disk electrodes via two procedures, A and B. Procedure A concerns liquids with insoluble breakdown products that settle from the space enclosed by disk electrodes in between breakdown tests, including petroleum oils, hydrocarbons, and askarels. In Procedure A, five breakdown tests are performed for every cup of liquid with tests conducted at 1-minute intervals. The mean of the five tests, known as the breakdown voltage, is calculated via the equation in Figure 1 and recorded to two significant figures. Meanwhile, Procedure B concerns liquids with insoluble breakdown products that do not completely settle from the space enclosed by disk electrodes in between breakdown tests and liquids without ASTM specifications. In Procedure B, one breakdown test for five different trials is performed with the mean of the five breakdowns, each recorded to two significant figures and calculated with the same equation in Procedure A. The breakdown voltage is found acceptable only if the range of the five breakdowns does not exceed 92% of the mean value. If the range exceeds that value, then five additional tests are performed. Afterwards, the mean of the ten breakdown tests should be determined to be less than 151% of the mean to be accepted. If the range exceeds the mean again, there is a non-negligible source of error that needs to be investigated before the procedure repeats.

$$\overline{X} = n^{-1}\left(\sum_{i=1}^{n} X_i\right)$$

Figure 1. Mean Dielectric Breakdown Voltage Formula[6]

Before testing, it is important to note that breakdown tests should utilize AC voltages with 45 to 65 Hz frequencies within a setting at 20 to 30°C . Sharp-edged electrodes of 25.4 mm diameter and 3.18 mm thickness should be mounted parallel to one another in the specimen cup, electrodes should be wiped clean before use or buffed and resurfaced at the sight of scratches, and the testing cup should be cleaned with a low-boiling solvent. Moreover, this test method is only effective in tests where voltages do not surpass 25 kV rms, the concentration of water in the specimen is no less than 60% saturated at room temperature, and specimen viscosity is not greater than 900 cSt at 40°C.

During testing, the electrodes should be 2.54 mm or 0.100 in apart using a 2.54 mm round gage, 2.53 mm thick flat steel go gage, or 2.55 mm thick flat steel no-go gage. Furthermore, the disk electrode edges' radii should be less than 0.010 in on the side with the gap against a 0.254 mm or 0.010 in radius gage with edges perpendicular to the face of the electrode. Figure 2 illustrates the scenarios for checking the edge radius. Figure 2a features a disk radius (gray area) equal to that of the gage

(white area) with both disk edges lining against the edges of the gage and the disk edge fitting perfectly in the gage radius, making the disk marginally acceptable due to possible deterioration. Figure 2b displays disk edges that extend past the gage edges with the disk edge not fitting into the gage radius, portraying an example of an unacceptable electrode. Lastly, Figure 2c shows one side of the disk edge lining up with one side of the gage edge while the sharp point of the disk fits into the gage radius with ample space at the other side of the disk edge, presenting an acceptable electrode.[6]

Figure 2a. Marginally Acceptable Electrode Edge[6]

Figure 2b. Unacceptable Electrode Edge[6]

Figure 2c. Acceptable Electrode Edge[6]

Dielectric Breakdown Tester K16185, K16186, K16187

Koehler Instrument Company's Dielectric Breakdown Tester (Figure 3) is compatible with the aforementioned test method. The instrument is complete with a thermal printer and 3.5" colored LCD display at the front panel, a high-voltage transformer, a measuring cell with high-voltage electrodes, high-voltage supply contacts that disconnects transformer voltages to the electrodes, adjustment wheels devised to adjust the space between electrodes, a stirring electric motor

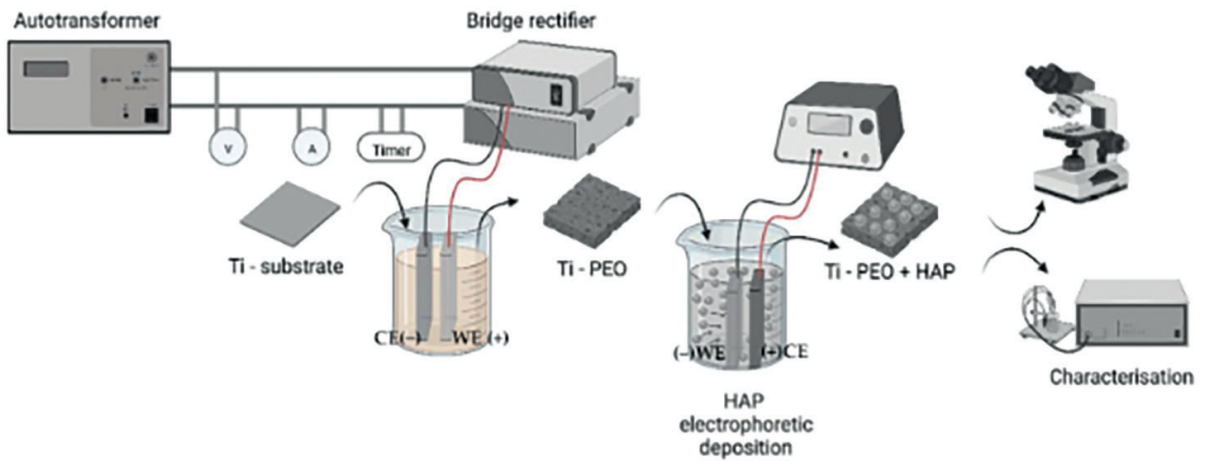

Figure 5. PEO Treatment of Ti and HAP Deposition Electrophoresis Procedure[8]

that torques the mechanical stirrer inside the measuring cell, and USB memory and power cable sockets at the front and rear panels as seen in the side cross-sectional diagram (Figure 4). In addition, this product offers two test template modes, standard and user-defined. Standard templates are pre-programmed settings that can only be edited by the manufacturer while user-defined templates offer adjustable test parameters, such as test counts, stirring time, delayed time between tests, and power frequencies ranging from 48 to 63 Hz with the touch of a button. All completed tests are then automatically archived with options to export files to a USB drive or print a test report detailing the date and time of test, test frequency, voltage increase rate (kV/s), sample temperature (°C), liquid type, average breakdown voltage, and standard deviation.[7]

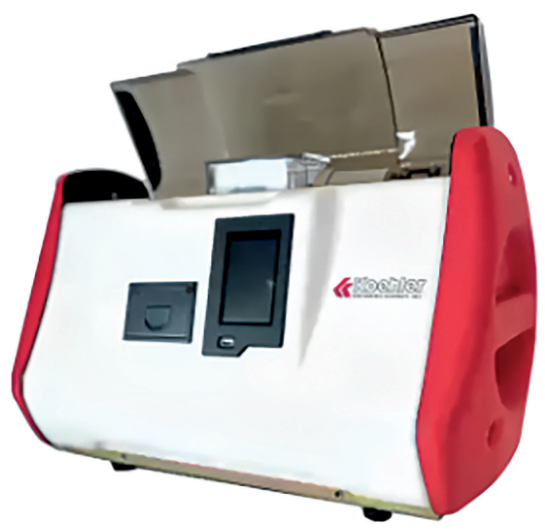

Figure 3. Koehler's Dielectric Breakdown Tester[7]

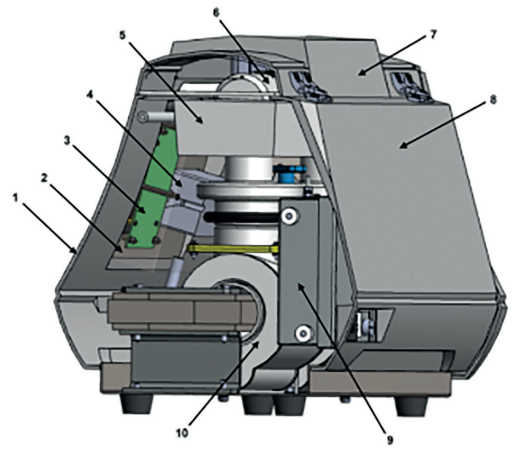

Figure 4. Side Interior View[7]

Titanium Coating Morphology with PEO

According to Muntean, Roxana, et al. from Politehnica University Timisoara in Romania, Titanium and its alloys are often used in engineering fields because of their high strength to weight ratio, corrosion resistance, and biocompatibility. Despite this, many concerns arise when titanium is employed in an aggressive environment that could affect its stability, wear resistance, and bond strength. Under natural conditions, titanium readily forms a stable 1.5 to 5.0 nm thin oxide layer. However, applied loads contacting its surface result in low oxygen conditions and damage or crevice corrosions to the oxide layer. Hence, plasma electrolytic oxidation (PEO), a common treatment method to enhance surface performance through growing an inert oxide layer, is a technique looked into that would hopefully combat this problem. The PEO process involves rendering the metal as the anode immersed in an electrolyte and directing a voltage value greater than that of the dielectric breakdown voltage of the oxide layer to construct a ceramic-like porous layer. The porous coating composes two layers, an outer layer covered in pores and cracks and a dense, more compact inner layer. PEO-developed coatings are rapid, eco-friendly metal modifications with high ductility, corrosion resistance, and biocompatibility that offers customizable thickness, porosity, and microstructures. Moreover, adding particles into the electrolyte solution or directly after the oxidation of the new layer could enhance the properties of the PEO-developed coating, amplifying its antifouling, adhesion, hardness, and wettability characteristics. In 2023, Muntean, Roxana, et al. attempted to evaluate the corrosion resistance and wearability of hydroxyapatite-modified titanium dioxide (TiO_2) produced via a two-step procedure, PEO treatment in sodium silicate and potassium hydroxide alkaline solution followed by incorporating hydroxyapatite particles (HAP).

Pure titanium sheets were cut into smaller rectangular shapes to be used as an anode in an alkaline electrolyte solution while a rectangular stainless steel plate acted as the cathode. Two trials were performed such that one used a direct current (DC) while the other used a pulsed current (PC), both at a value of 200 mA and a maximum voltage of 240 V. Afterwards, the PC PEO-treated samples were washed with distilled water and dried before the addition of HAP. The Ti PC PEO samples were subjected to HAP deposition electrophoresis, an process that separates charged particles in liquids via electric fields, by suspending the Ti PC PEO samples (cathode) and a graphite plate (anode) in a HAP and isopropanol solution. Three trials per sample were conducted before surface roughness, corrosion resistivity, and wear characters were tested. Outline of the full experimental procedure is illustrated in Figure 5.

Figure 6 compares the surfaces of Ti PEO DC (a), Ti PEO PC (b), and Ti PEO PC + HAP (c). As the induced voltage approached the breakdown voltage of the original film layer during PEO treatment, sparking phenomena, discharge channels, and oxidation and melting processes occur. The molten oxides produced from oxidation and melting travel from the coating surfaces and through discharge channels before cooling, creating uneven micropores as craters. Ti PEO DC observed several open pores and irregularities with the highest average roughness and thickness values of 0.4 µm and 35 µm, respectively, as the result of intense gas evolution or release of during film oxidation partnered with intense heating associated with DC that melt and eject oxides from the coatings. Conversely, Ti PEO PC noticed a smoother, denser, and less porous surface with average roughness and thickness values reaching 0.3 µm and 12 µm, respectively. The pauses between current pulses in PC prevented surface overheating, well-controlled discharge intensities, and limited gas evolutions, an ideal method for adjusting coating roughness and thickness. Meanwhile, Ti PEO PC with HAP electrophoresis deposition saw uniform distribution of HAP (bright specks in Figure 6c) that filled in surface cavities with the second lowest roughness value of 0.2 µm and a thickness value of 16 µm. The Ti substrate had the smoothest surface with a recorded roughness value of 0.15 µm and a relative surface thickness of 0 µm since it did not undergo PEO treatment.

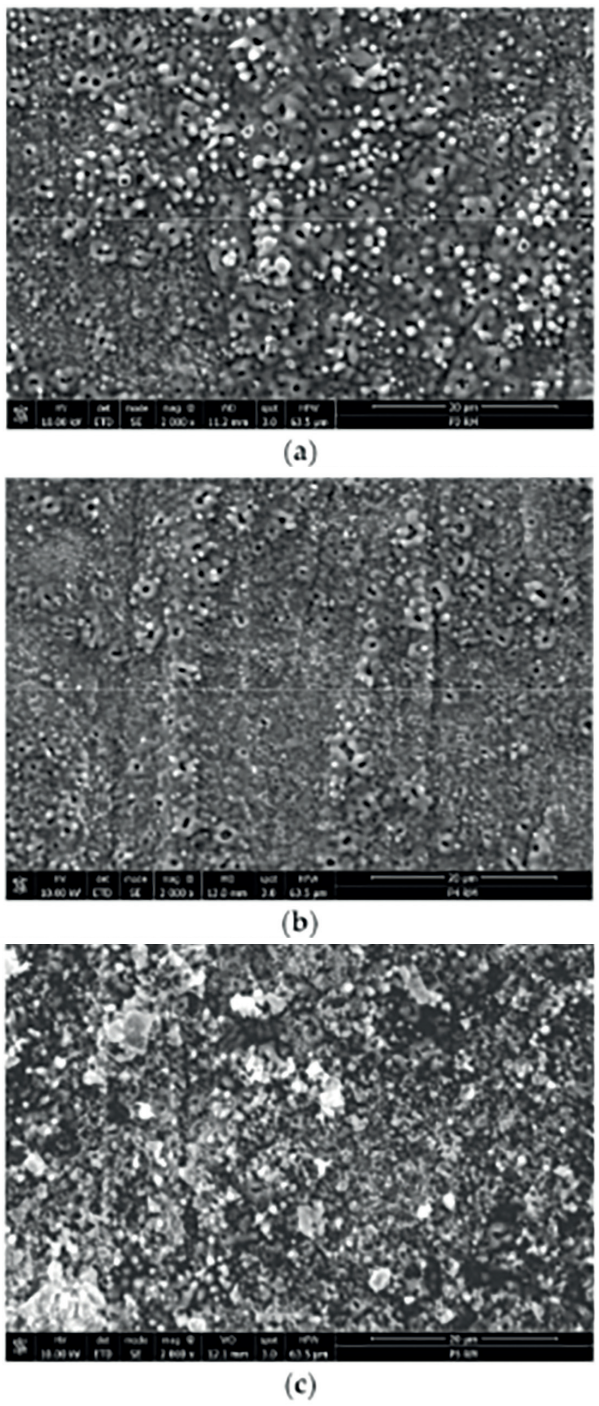

Figure 6. Ti Samples' Surfaces: Ti PEO DC (a), Ti PEO PC (b), and Ti PEO PC + HAP (c)[8]

To assess the corrosion resistance of the samples, electrochemical impedance spectroscopy (EIS) was performed. Figure 7a summarizes the EIS data collected from the samples, labeling resistance values for the outer (R_1) and inner (R_2) coating layers in Ω cm^2, associated percent error in every measurement, and a goodness-of-fit value indicated by the Chi-squared value x^2 (lower values of x^2 corresponds to closer proximity between experimental and expected data). The inner layers of Ti PEO DC and Ti PEO PC were two orders of magnitude greater than that of the outer layer while the inner layer of Ti PEO PC + HAP expressed a three orders of magnitude increase, implying that the inner layer was mainly responsible for the corrosion resistance in PEO-developed coatings. Corrosion resistance values of the inner layer increases in the order of Ti substrate (without PEO) < Ti PEO PC < Ti PEO PC + HAP < Ti PEO DC with values of 1.2x10^4 Ω cm^2, 0.29x10^6 Ω cm^2, 5.02x10^6 Ω cm^2, and 8.14x10^6 Ω cm^2, respectively. Minimal improvement in resistance value was seen with the addition of HAP, but higher corrosion resistance in PEO coatings was connected to increased coating thickness. To better visualize the resistance values of the inner and outer layers of the Ti samples, bar graphs (Figure 7b and 7c) for each layer were constructed with resistance values expressed in 10^4 Ω cm^2 and marked percent error bars according to Figure 7a. .

Finally, to determine the wear rate of the samples, the change in coefficient of friction (COF) between a 5N-100Cr100 ball and the titanium sheets beneath it over a sliding distance of 1000 meters over time was examined. Figure 8 graphs each sample's evolution of COF against the distance traveled as the ball revolves at a rate of 300 revolutions per minute. For all the samples, the first 250 meters exhibited the greatest variation in COF before settling to a higher, constant value throughout the rest of the distance. The Ti substrate was

Parameter	Ti Substrate	Ti PEO DC	Ti PEO PC	Ti PEO PC + HAP
R_S/Ω	31.8 (0.7%)	20.6 (0.7%)	32.6 (1.5%)	30.6 (2.7%)
CPE-T_1/F cm^{-2} s^{n-1}	-	4.18×10^{-7} (3.7%)	5.20×10^{-6} (7.03%)	1.41×10^{-6} (7.3%)
n_1	-	0.69 (1.4%)	0.67 (1.1%)	0.70 (1.0%)
R_1/Ω cm^2	-	11.6×10^4 (6.9%)	0.25×10^4 (3.1%)	0.40×10^4 (2.4%)
CPE-T_2/F cm^{-2} s^{n-1}	4.35×10^{-5} (1.0%)	5.42×10^{-6} (4.9%)	3.54×10^{-5} (1.2%)	7.30×10^{-6} (1.0%)
n_2	0.91 (0.2%)	0.66 (5.6%)	0.78 (1.0%)	0.86 (0.5%)
R_2/Ω cm^2	1.2×10^4 (0.9%)	8.14×10^6 (88%)	0.29×10^6 (5.7%)	5.02×10^6 (11.5%)
χ^2	2.5×10^{-3}	1.9×10^{-2}	4.5×10^{-3}	5.1×10^{-3}

Figure 7a. EIS Data of Ti Samples[8]

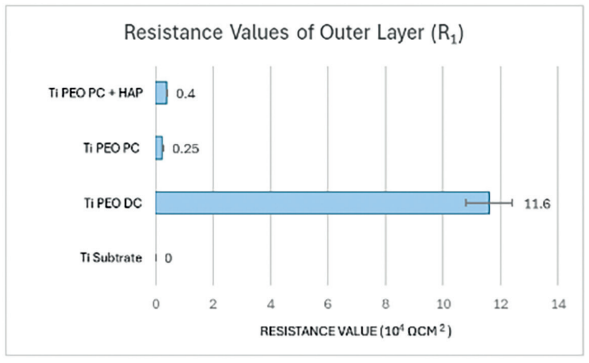

Figure 7b. Bar Graph Analysis of Outer Layer's Resistance Values (10^4 Ωcm^2)

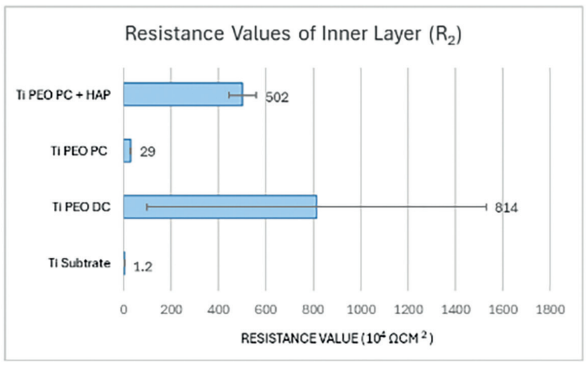

Figure 7c. Bar Graph Analysis of Inner Layer's Resistance Values (10^4 Ωcm^2)

noted with poor mechanical properties, low hardness, and high wear rate due to it obtaining the lowest starting COF of 0.2 and lowest maximum COF of 0.65, explained by its smooth surface characteristic. On the other hand, both DC and PC Ti PEO began with a COF of 0.5 and ended with an average COF of 0.8 because of their rough, porous coating increasing friction forces and friability of the outer layer. With the PC Ti PEO + HAP, its COF closely resembled that of the Ti substrate, beginning with a much lower COF of 0.33 and the same maximum COF of 0.65. The addition of HAP decreases surface roughness by filling in crevices and constructs a tribofilm against external contacts that mitigates friction. With the measured COF across all samples, wear rates (10^4 mm^3 N^{-1} m^{-1}) were ascertained and plotted in a bar graph in Figure 9. Although both DC and PC Ti PEO showed higher COF than that of the Ti substrate, wear rate was estimated to be 50% less than that of the Ti substrate. Meanwhile, the Ti substrate and PC Ti PEO + HAP, samples of the smoothest surfaces, had the highest wear rates with PC Ti PEO + HAP having a slightly lower rate than that of the Ti substrate.

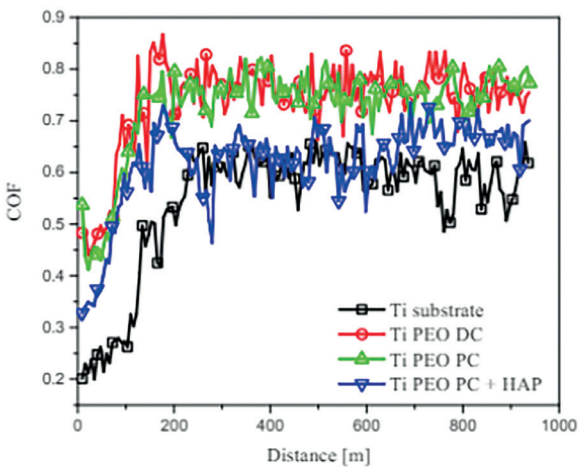

Figure 8. Change in COF vs. Travel Distance Graph[8]

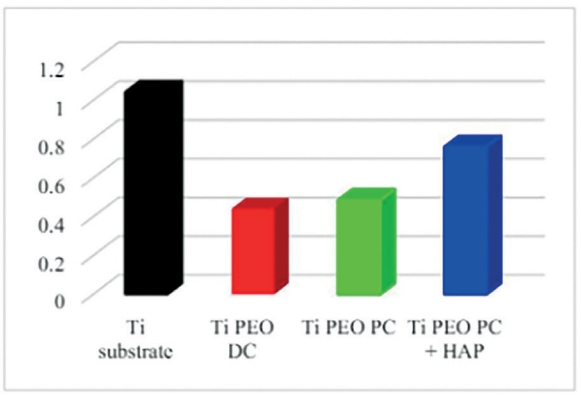

Figure 9. Wear Rates of Ti Samples[8]

Ultimately, the surface roughness, corrosion resistance, and wearability tests executed point towards the conclusion that PEO coatings entirely outperform regular Ti substrates. PEO has proven successful in transfiguring titanium coating, a new application pivoting off the stereotypically avoided dielectric breakdown of a film layer, and can function as a potential solution to many engineering obstacles.[8]

Digital Fingerprints from Breakdown Spots

According to Porti, Marc, et al. from the Autonomous University of Barcelona, Spain, dielectric breakdown (BD) of the gate oxide in Metal-Insulator-Semiconductor (MIS) or Metal-Insulator-Metal (MIM) capacitors is notorious for possible percolation, short circuits, micro-explosions, crater marks on electrodes, and irreversible damages. Regardless, BD occurs randomly on a nanoscale level as BD spots, which are detectable through optical microscopes. Hence, entropy in dielectric breakdowns have been studied and used as a source for cryptography, security, and Physically Unclonable Functions (PUFs), functions responsible for generating irreproducible fingerprints and image processing in sectors of identification, authentication, and anti-counterfeiting, within past years. In 2023, Porti, Marc, et al. attempted to create PUFs using the spatial distribution of BD spots in Pt/HfO_2/Pt MIM capacitors manufactured on top of a SiO_2 layer and Si substrate. The fabrication of cryptographic keys in this case included collecting optical images of the MIM capacitors after experiencing dielectric breakdown, binarizing the optical image for better sensitivity of BD spots, debiasing the images to eliminate repetition, and converting the first 256 bits of each image to generate a key map as detailed in Figure 10.

Figure 11a outlines the cross-section of a MIM capacitor, consisting of a dielectric HfO2 layer interjected between two Pt electrode layers, on top of SiO2 and Si substrate layers. Figure 11b captures a top profile image of a one of the nine MIM capacitors samples tested after dielectric breakdown. The 500 µm square capacitor endured the electric stress of -9 V for 60 seconds before breaking down, producing dispersed tiny, black dots representing random BD spots on the top electrode layer. Figure 12a displays two optical images of two different MIM capacitors after their dielectric breakdown phase and their relative binarized images in Figure 12b, in which each white spot corresponds to a BD spot. Prior to binarization, the optical images were separated into three 2D matrices, each matrix comparing RGB (red, green, blue) colors. Afterwards, these matrices were scaled from 0 to 1 and individually assigned a threshold value to be binarized (0.9, 0.9, and 0.2 for red, green, blue, respectively).

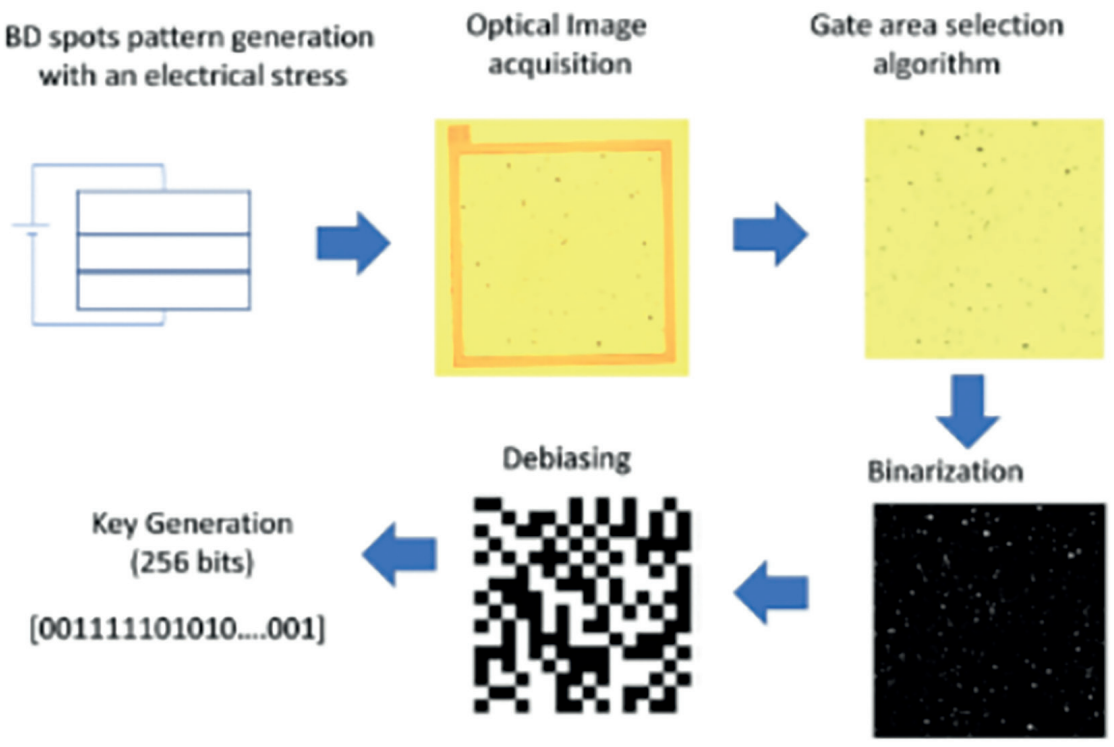

Figure 10. Creation of PUFs from BD Spots Patterns Flowchart[9]

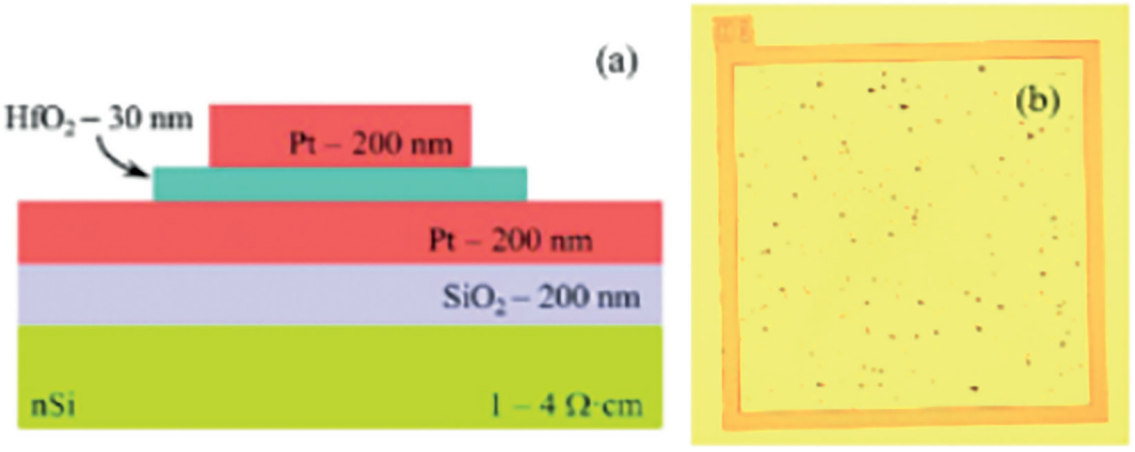

Figure 11. Cross Section of MIM Capacitor (a) BD Spots Pattern of MIM Capacitor (b)[9]

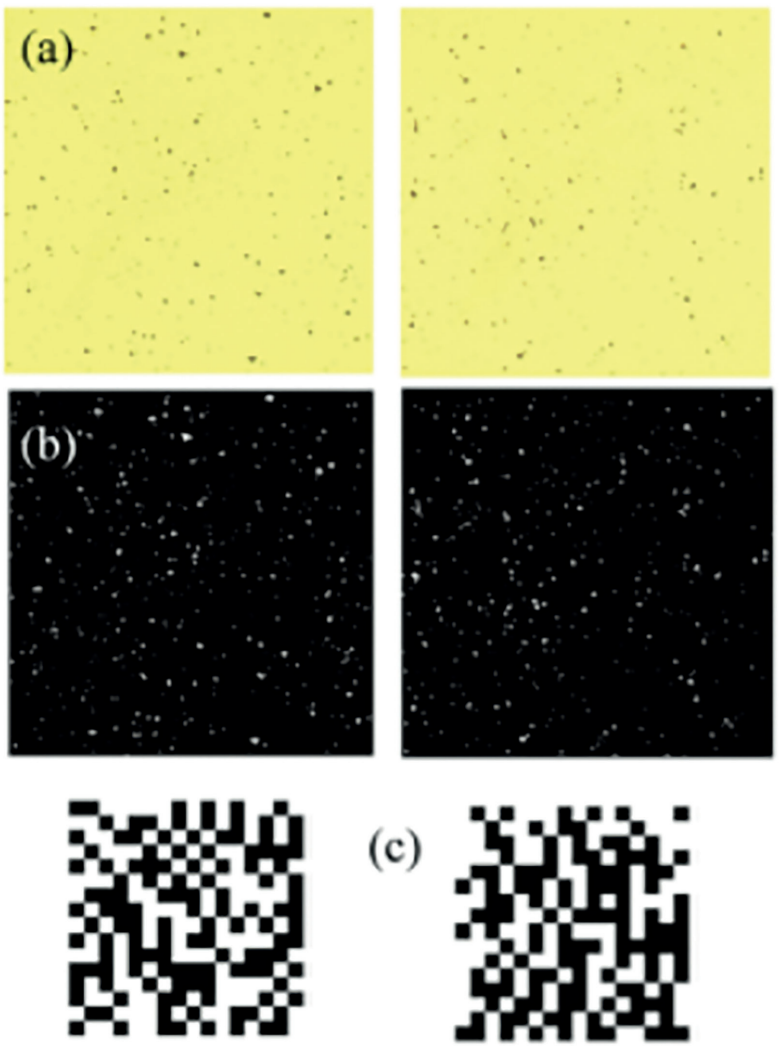

Figure 12. Optical Images of Two Separate MIM Capacitors (a) Binarized Images (b) Cryptographic Keys (c)[9]

1 represents a BD spot (white) while 0 indicates the absence of it (black), with colors specially chosen to improve visual detection. Once a binarized image forms, the debiasing method was implemented to remove errors in the amount of 0s and 1s reached and reformatted the binary numbers into bits. Lastly, the first 256 bits of each image were used to create a cryptographic key as a 16x16 pixels map seen in Figure 12c.

Following up on the experiment, the quality of the cryptographic keys was analyzed by assessing their uniformity, uniqueness, and reproducibility. Uniformity was measured by dividing the number of 0-bits by the total number of bits with the ideal distribution rate of 50%. Here, the mean uniformity value of all nine MIM capacitors was 50.4% with a 1.67% standard deviation, relatively close to the ideal value. Next, device uniqueness was found by comparing Hamming Distance (HD), or the number of different bits between two keys with respect to the total number of bits. The average inter-device HD value was 49.72% with 3.37% standard deviation, also fairly close to the ideal 50% value. Finally, reproducibility of the same key using different images of the same capacitor was also determined. The same procedure was performed 1.5 months later on the same capacitor and intra-HD distance of their keys was compared to locate the number of changed bits. With all nine capacitors, mean device reproducibility was 98.82% with 0.89% standard deviation, a finding astoundingly close to the ideal value of 100%. In the end, the study introduces an atypical route for the generation of PUFs through the analysis of breakdown spot spatial patterns in MIM capacitors with met uniformity, uniqueness, and reproducibility criteria and puts forth another potential application of dielectric breakdowns in the collaborative fields of electronics and cybersecurity that challenges our conventional norms.[9]

Conclusion

Since the late eighteenth century, a myriad of industries have been incorporating dielectrics into their productions for its polarizable, insulating qualities and vehemently forewarned users of its breakdown and ionization hazards. While it is necessary to determine the breakdown voltage of dielectric materials via ASTM testing, it is also imperative to recognize the many rewarding applications of dielectric breakdowns in grander processes as described in recent studies of plasma electrolytic oxidation treatment for enhanced titanium coating and the buildings of highly reliable cryptographic keys using random breakdown spot patterns. Hopefully, modern research will convince industries to engender a fresh outlook on the practicalities of dielectric breakdowns and employ their functions on a grandiose scale.

Work Cited

[1] James, Olivia. "A Brief Note on Dielectric Materials." Global Science Research Journals, 2022, https://www.globalscienceresearchjournals.org/articles/a-brief-note-on-dielectric-materials-86972.html.

[2] "Dielectric Materials." EETech Group, https://eepower.com/capacitor-guide/fundamentals/dielectric-materials/#.

[3] Brown, William D. et al. "The Electrochemistry Society Interface." The Electrochemistry Society, Inc., vol. 15, no. 1, 2006, https://knowledge.electrochem.org/encycl/art-d01-dielectrics.htm.

[4] "Electrical Breakdown." Elsevier, https://www.sciencedirect.com/topics/materials-science/electrical-breakdown#:~:text=2.4%20Dielectric%20breakdown&text=This%20occurs%20when%20at%20a,state%20of%20internal%20thermal%20equilibrium.

[5] "Dielectric Breakdown." University of Cambridge, https://www.doitpoms.ac.uk/tlplib/dielectrics/breakdown.php.

[6] "Standard Test Method for Dielectric Breakdown Voltage of Insulating Liquids Using Disk Electrodes." ASTM International, 31 Dec. 2010, https://www.astm.org/d0877-00.html.

[7] "Automatic Dielectric Breakdown Tester." Koehler Instrument Company, Inc., 2024, https://koehlerinstrument.com/products/automatic-dielectric-breakdown-analyzer/?search=dielectric&description=true&sub_category=true.

[8] Muntean, Roxana, et al. "Characteristics of Hydroxyapatite-Modified Coatings Based on TiO2 Obtained by Plasma Electrolytic Oxidation and Electrophoretic Deposition." Materials, vol. 16, no. 4, 2023, pp. 1410-, https://doi.org/10.3390/ma16041410.

[9] Porti, Marc, et al. "Oxide Breakdown Spot Spatial Patterns as Fingerprints for Optical Physical Unclonable Functions." IEEE Electron Device Letters, vol. 44, no. 10, 2023, pp. 1–1, https://doi.org/10.1109/LED.2023.3301974.

About the Authors

Dr. Raj Shah a Director at Koehler Instrument Company in New York, where he has worked for the last 28 years. He is an elected Fellow by his peers at IChemE, CMI, STLE, AIC, NLGI, INSTMC, AOCS, Institute of Physics, The Energy Institute and The Royal Society of Chemistry. An ASTM Eagle Award recipient, Dr. Shah recently coedited the bestseller, "Fuels and Lubricants Handbook," details of which are available at "ASTM's Long-Awaited Fuels and Lubricants Handbook 2nd Edition Now Available" (https://bit.ly/3u2e6GY). He earned his doctorate in

Chemical Engineering from Pennsylvania State University and is a Fellow of The Chartered Management Institute, London. Dr. Shah is also a Chartered Scientist with the Science Council, a Chartered Petroleum Engineer with the Energy Institute and a Chartered Engineer

with the Engineering Council, UK. Dr. Shah was recently granted the honorific of "Eminent Engineer" with Tau Beta Pi, the largest engineering society in the USA. He is on the Advisory Board of Directors at the State University of New York, Farmingdale (Mechanical Technology

and Engineering Management); Auburn University (Tribology); and the State University of New York, Stony Brook (Chemical Engineering/Materials Science and Engineering). An Adjunct Professor at Stony Brook University, in the Department of Materials Science and

Chemical Engineering, Raj also has over 650 publications and has been active in the energy industry for over 3 decades.

More information on Raj can be found at https://bit.ly/3QvfaLX.

Contact: rshah@koehlerinstrument.com

Ms. Rachel Ly is part of a thriving internship program at Koehler Instrument Company in Holtsville and is a student of Chemical Engineering at Stony Brook University, Long Island,

NY, where Dr. Shah is the current chair of the external advisory board of directors.

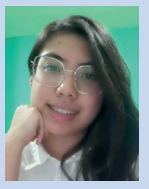

Rachel Ly

Author Contact Details

Dr. Raj Shah, Koehler Instrument Company • Holtsvile, NY11742 USA • Email: rshah@koehlerinstrument.com

• Web: www.koehlerinstrument.com